Sensors & Transducers, Vol. 160, Issue 12, December 2013, pp. 176-183

www.sensorsportal.com

Sensors & Transducers

http://www.sensorsportal.com

Performance Analysis of Magnetostrictive Cantilever Beam with Modeling

[1, 2, 3] Qinghua CAO, [2] Dingfang CHEN, [2] Chuan LI, [3] Quanguo LU, [3] Jianwu YAN

[1] School of Automation, Wuhan University of Technology, 430083,Wuhan, China
[2] Institute of Intelligent Manufacturing and Control, Wuhan University of Technology, 430063, Wuhan, China
[3] Institute of Micro/nano Actuation and Control, Nanchang Institute of Technology, 330099, Nanchang, China

Received: 25 September 2013 /Accepted: 22 November 2013 /Published: 30 December 2013

Abstract: A magnetostrictive cantilever beam model is established by combining an energy-based constitutive magnetostrictive model with the classical Euler-Bernoulli beam theory constitutive relations that describe the material behavior are based on energy minimization techniques. We use the saturation magnetization, the magnetostrictive constant and the 4th and 6th order anisotropy constants to calculate the Zeeman, stress-induced anisotropy and magnetocrystalline anisotropy energies per unit volume. The stress of the magnetostrictive cantilever beam is solved by classical beam theory. Experiments and simulations are conducted to study performance of the cantilever. The results demonstrated the sensing is primarily due to the dominating effect of compression over tension. A critical bias magnetic field is required below which the magnetostrictive sensing cannot be observed under bending. *Copyright © 2013 IFSA.*

Keywords: Magnetostrictive, Beam, Modeling, Magnetization.

1. Introduction

Iron–gallium alloys (galfenol) exhibit moderate magnetostriction (~350 ppm) under very low magnetic fields ~100 Oe (8000 A m^{-1}), have very low hysteresis, and demonstrate high tensile strength (~500 MPa) and limited variation in magnetomechanical properties for temperatures between −20 and 80 °C [1-5]. These materials are, in general, machinable, ductile and can be welded. Thus, they can be easily threaded, attached to existing structures and used as load bearing members. They have a high Curie temperature (675 °C) and are corrosion resistant. The raw materials used to produce FeGa alloys are relatively inexpensive. All these factors demonstrate that FeGa alloys have great promise as an engineering material for actuation and sensing applications [6-7].

Yoo designed a tuning fork-based gyro sensor which uses mm-size Galfenol patches as actuator and sensor material in bending [8]. Downey showed that mm-scale Galfenol rods can be used as a sensor in bending and the results of this work was used to conceptualize a nanowire-based broadband acoustic sensor [9]. Further work in this area led to the mechanical characterization of Galfenol nanowires which showed that although their Young's modulus is similar to that of bulk material, they possess almost three times the tensile strength. Datta and Flatau showed that Galfenol could be adhered to a structural

material and used as strain sensor in bending [10]. Hale and Flatau and Parsons demonstrated the application of Galfenol in tactile sensing and torque sensing respectively. Ghodsi developed a positioning actuator for cryogenic environment. Ueno et al. developed linear actuator, wobbler and vibrator [11-13].

Such applications motivate the development of a modeling framework and performance analysis for active structures. Structural modeling of extensional magnetostrictive transducers has successfully been performed, while performance analysis of Magnetostrictive cantilever has been a challenge.

Various non-linear models have also been developed to account for the magnetomechanical response of ferromagnetic materials over different operating conditions. Higher order series expansion of the free energy yielded the Landau model. Bergqvist and Engdahl combined the effects due to stress and magnetic field into an equivalent field term and incorporated this in the Preisach operator to model the effect of stress on magnetization. A stress-induced field term was introduced into the Langevin term by Jiles to model the effect of stress on magnetization vs. field curves as well as the effect of magnetic field on magnetization vs. stress curves . Ghosh and Gopalakrishnan used a neural network technique to non-linearize the coupled constitutive equations and successfully predicted both the actuation and sensing characteristics of magnetostrictive materials. These models were limited to one-dimensional analysis and did not account for magnetocrystalline anisotropy which is required to capture the directional preference of magnetization orientation based on the crystal symmetry of different materials.

Armstrong extended the Stoner-Wohlfarth model to cubic anisotropy and was able to come up with a three-dimensional model for magnetostrictive actuation [14]. This approach was adapted to model both the actuator and predict the sensor responses of single crystal and polycrystalline Galfenol subjected to collinear stress and magnetic fields. An extension to this approach was developed to add stress-annealing effect by incorporating a uniaxial anisotropy. These models included Zeeman, stress-induced anisotropy and magnetocrystalline anisotropy energy but excluded the exchange energy because it is non-zero only within the domain wall and hence forms a small fraction of the total energy of a bulk sample. Moreover, the preclusion of the magnetostatic energy incapacitates the ability of these models to account for demagnetization effects.

Smith developed a homogenized energy model which included magnetostatic, stress-induced anisotropy, magnetocrystalline anisotropy and exchange energy terms [11]. The exchange interaction was phenomenologically incorporated using Boltzmann statistics which ironically considers only noninteracting particles. Moreover the use of Boltzmann statistics is only applicable to a large number of particles and may not be a valid assumption near saturation when the material is almost in a single domain state. Using Armstrong's energy formulation and Smith's framework of homogenized energy model, Dapino developed a magnetomechanical model which takes into account six possible directions of magnetization orientation instead of two directions in Smith's work [1]. These approaches introduce dynamic effects into the constitutive model using thermal relaxation techniques and are particularly useful for obtaining closed minor loops when operating an actuator or sensor with DC bias magnetic field and stress respectively.

This article investigates the performance analysis of Galfenol-driven cantilever beam considering the effect of the magnetic induction and stress. In order to motivate a modeling technique in the frame, a magnetostrictive cantilever beam model is established, constitutive relations that describe the material behavior are based on energy minimization techniques. We use the saturation magnetization (Ms), the magnetostrictive constant (λ_{100}) and the 4th and 6th order anisotropy constants (K_1 and K_2 respectively) to calculate the Zeeman, stress-induced anisotropy and magnetocrystalline anisotropy energies per unit volume. We adopt the Euler-Bernoulli assumptions of the Classical Beam Theory to solve stress of the magnetostrictive cantilever beam. Experiments and simulations are conducted to study performance of the cantilever. The experiments and results are presented next, followed by concluding remarks.

2. Fundamental Relations in Magnetostriction

The magnetocrystalline anisotropy energy per unit volume is expressed using phenomenological expressions which are suitable to account for the symmetry. For a cubic crystal, this energy can be approximated using equation (1):

$$E_{an} = K_1\left(\alpha_1^2\alpha_2^2 + \alpha_2^2\alpha_3^2 + \alpha_3^2\alpha_1^2\right) + K_2\alpha_1^2\alpha_2^2\alpha_3^2, \quad (1)$$

Here $\alpha_1 = \sin\theta\cos\phi, \alpha_2 = \sin\theta\sin\phi$ and $\alpha_3 = \cos\theta$ are the direction cosines of the magnetization ($M = M_s\alpha$) with respect to the three cube edges and K1 and K2 are the 4th and 6th order anisotropy constants respectively. Based on a spherical coordinate system, $0 \le \theta \le \pi$ and $0 \le \varphi \le 2\pi$.

The dipole-dipole interaction energy between the atoms shown in Fig. 1 can be modeled using Equation (2) where r is the bond length, $[\alpha_1, \alpha_2, \alpha_3]$ are the magnetization direction cosines

as defined in Equation (1) and $[\beta_1, \beta_2, \beta_3]$ are the direction cosines of the bond direction.

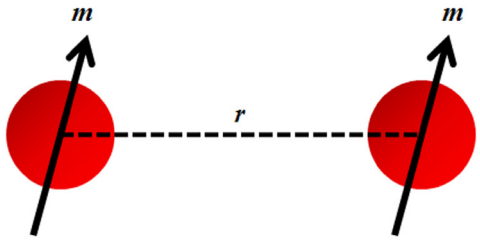

Fig. 1. A one-dimensional representation of interaction between neighboring dipoles with magnetic moment m separated by bond length r.

$$w(r,a) = l(r)\left\{(\alpha_1\beta_1 + \alpha_2\beta_2 + \alpha_3\beta_3)^2 - \frac{1}{3}\right\}, \quad (2)$$

When the crystal is strained, the bond length and consequently the interaction energy change. The sum of the change in the interaction energy for the nearest neighbor pairs can be expressed as Equation (3) where the tensor $[\varepsilon_{11}, \varepsilon_{22}, \varepsilon_{22}, \varepsilon_{23}, \varepsilon_{31}, \varepsilon_{12}]$ describes the strain in the crystal. The term E_{magel} is the magnetoelastic energy.

$$\begin{aligned} E_{magel} = b_1\left\{\varepsilon_{11}\left(\alpha_1^2 - \frac{1}{3}\right) + \varepsilon_{22}\left(\alpha_2^2 - \frac{1}{3}\right) + \varepsilon_{33}\left(\alpha_3^2 - \frac{1}{3}\right)\right\}, \\ + b_2\left(\varepsilon_{23}\alpha_2\alpha_3 + \varepsilon_{31}\alpha_3\alpha_1 + \varepsilon_{12}\alpha_1\alpha_2\right) \end{aligned} \quad (3)$$

The coefficients b_1 and b_2 are known as magnetoelastic coupling coefficients. They depend on the number of nearest neighbor pairs, unstrained bond length, the function $l(r)$ and its spatial gradient. The spontaneous magnetostriction or equilibrium strain in a domain in the absence of any external stress or magnetic field can be obtained by minimizing the sum of magnetoelastic and elastic energy with respect to each of the strain components. The expression for elastic energy in a cubic crystal is shown in Equation (4) where c_{11}, c_{12} and c_{44} are the elastic constants.

$$\begin{aligned} E_{el} &= \frac{1}{2}c_{11}\left(\varepsilon_{11}^2 + \varepsilon_{22}^2 + \varepsilon_{33}^2\right) \\ &+ \frac{1}{2}c_{44}\left(\varepsilon_{23}^2 + \varepsilon_{31}^2 + \varepsilon_{12}^2\right) \\ &+ c_{12}\left(\varepsilon_{22}\varepsilon_{33} + \varepsilon_{33}\varepsilon_{11} + \varepsilon_{11}\varepsilon_{22}\right) \end{aligned}, \quad (4)$$

The magnetostriction tensor $\left[\tilde{\lambda}\right]$ are shown in Equation (5).

$$\left[\tilde{\lambda}\right] = \begin{bmatrix} \lambda_{11} \\ \lambda_{22} \\ \lambda_{33} \\ \lambda_{23} \\ \lambda_{31} \\ \lambda_{12} \end{bmatrix} = \begin{bmatrix} \frac{b_1}{c_{12}-c_{11}}\begin{Bmatrix} \left(\alpha_1^2 - \frac{1}{3}\right) \\ \left(\alpha_2^2 - \frac{1}{3}\right) \\ \left(\alpha_3^2 - \frac{1}{3}\right) \end{Bmatrix} \\ -\frac{b_2}{c_{44}}\begin{Bmatrix} \alpha_2\alpha_3 \\ \alpha_3\alpha_1 \\ \alpha_2\alpha_2 \end{Bmatrix} \end{bmatrix}, \quad (5)$$

The strain along the direction cosines $[\beta_1, \beta_2, \beta_3]$ can be expressed by Equation (6)

$$\begin{aligned} \varepsilon_{[\beta_1,\beta_2,\beta_3]} &= \varepsilon_{11}\beta_1^2 + \varepsilon_{22}\beta_2^2 + \varepsilon_{33}\beta_3^2, \\ &+ \varepsilon_{23}\beta_2\beta_3 + \varepsilon_{31}\beta_3\beta_1 + \varepsilon_{12}\beta_1\beta_2 \end{aligned} \quad (6)$$

The magnetostriction along [100] which is shown in Equation (7) can be obtained by substituting $\alpha_1 = \beta_1 = 1$ and $\alpha_2 = \beta_2 = \alpha_3 = \beta_3 = 0$ in Equations (5) and (6).

$$\lambda_{100} = \frac{2}{3}\frac{b_1}{(c_{12}-c_{11})} = -\frac{1}{3}\frac{b_1}{c'}, \quad (7)$$

Similarly the magnetostriction along which is shown in Equation (8) can be obtained by substituting $\alpha_1 = \beta_1 = \alpha_2 = \beta_2 = \alpha_3 = \beta_3 = 1/\sqrt{3}$ in Equations (4) and (6).

$$\lambda_{111} = -\frac{1}{3}\frac{b_2}{c_{44}}, \quad (8)$$

Combining Equations (5)-(8), the magnetostriction along any arbitrary direction $[\beta_1, \beta_2, \beta_3]$ can be expressed using Equation (9) when the magnetization direction is along $[\alpha_1, \alpha_2, \alpha_3]$.

$$\begin{aligned} \lambda_{\beta_1\beta_2\beta_3} &= \frac{3}{2}\lambda_{100}\left(\alpha_1^2\beta_1^2 + \alpha_2^2\beta_2^2 + \alpha_3^2\beta_3^2 - \frac{1}{3}\right), \\ &+ 3\lambda_{111}\left(\alpha_2\alpha_3\beta_2\beta_3 + \alpha_3\alpha_1\beta_3\beta_1 + \alpha_1\alpha_2\beta_1\beta_2\right) \end{aligned} \quad (9)$$

If the equilibrium strains from Equation (5) are substituted back in Equations (4) and (3), the sum of the magnetoelastic and elastic energies would translate into an equivalent 4th order magnetostrictive anisotropy energy which can be expressed by Equation (10). The coefficient is following.

$$E_{\Delta K_1} = \Delta K_1\left(\alpha_1^2\alpha_2^2 + \alpha_2^2\alpha_3^2 + \alpha_3^2\alpha_1^2\right), \quad (10)$$

Hence the effective magnetocrystalline anisotropy is given by the sum of Equations (1) and (10). It should be noted that measured values of K_1 include the value ΔK_1 as the magnetostrictive anisotropy (ΔK_1) cannot be experimentally distinguished from the pure magnetocrystalline anisotropy (K_1).

3. Modeling of Constitutive Behavior

Constitutive relations that describe the material behavior are usually based on energy minimization techniques. The first part of such a technique involves the formulation of an energy functional which includes or precludes certain terms based on assumptions appropriate for the purpose of the model. The second part involves the use of mathematical techniques to extract the information about a required physical response of the material under the influence of force fields that perturb the energy.

The simplest model for magnetoelastic material is the coupled linear constitutive equations. Considering both strain and magnetic induction in the material as functions of stress and magnetic field, a first order truncated Taylor series expansion about a given operating point (H_0, σ_0) can be written as Equations (11) and (12). Note that stress and magnetic field are assumed to be independent inputs to the material.

$$d\varepsilon = \left.\frac{\partial \varepsilon}{\partial \sigma}\right|_{H_0,\sigma_0} d\sigma + \left.\frac{\partial \varepsilon}{\partial H}\right|_{H_0,\sigma_0} dH \quad , \tag{11}$$

$$dB = \left.\frac{\partial B}{\partial \sigma}\right|_{H_0,\sigma_0} d\sigma + \left.\frac{\partial B}{\partial H}\right|_{H_0,\sigma_0} dH \quad , \tag{12}$$

The following Gibb's free energy formulation can be used to couple Equations (11) and (12) and also to provide physical interpretations of the differential quantities. The total work done (dW) on a unit volume of ferromagnetic material by a stress and magnetic field due to infinitesimal change in strain and magnetic induction can be expressed by Equation (13). Note that dW is not an exact differential.

$$dW = \sigma d\varepsilon + HdB \quad , \tag{13}$$

For a reversible process, the change in internal energy (dU) can be expressed using Equation (14) which can be obtained by substituting Equation (13) in the 1st Law of Thermodynamics. Here S and T denote entropy and temperature respectively.

$$dU = \sigma d\varepsilon + HdB + TdS \quad , \tag{14}$$

The Gibb's free energy of the system is given by Equation (15)

$$G = U - \sigma\varepsilon - HB - TS \quad , \tag{15}$$

The change in Gibb's free energy in an isothermal reversible process can be expressed by Equation (16).

$$dG = dU - \varepsilon d\sigma - \sigma d\varepsilon - BdH - HdB - TdS, \tag{16}$$

Combining Equations (14) and (16), the change in Gibb's free energy can be written as shown in Equation (17).

$$dG = -\varepsilon d\sigma - BdH \quad , \tag{17}$$

Equation (17) can be used to interpret the differential quantities in Equations (11) and (12) as follows. The mechanical compliance of the material in a process where the magnetic field (H0) is maintained constant while the stress is quasistatically perturbed about a given stress σ_0 is expressed by Equation (18).

$$\left.\frac{\partial \varepsilon}{\partial \sigma}\right|_{H_0,\sigma_0} = -\left.\frac{\partial^2 G}{\partial \sigma^2}\right|_{H_0,\sigma_0} = S^{H_0,\sigma_0} \quad , \tag{18}$$

Similarly, magnetic permeability of the material in a process where the stress σ_0 is maintained constant while the magnetic field is quasi-statically perturbed about a given field (H0) is expressed by Equation (19).

$$\left.\frac{\partial B}{\partial H}\right|_{H_0,\sigma_0} = -\left.\frac{\partial^2 G}{\partial H^2}\right|_{H_0,\sigma_0} = \mu^{H_0,\sigma_0} \quad , \tag{19}$$

The strain coefficient ($d = \partial\varepsilon/\partial H$) and stress sensitivity ($d^* = \partial B/\partial\sigma$) which couple the effects of magnetic field and mechanical stress are expressed by Equations (20) and (21) respectively and are identical to each other as evident from their relation to the 2nd derivative of the Gibb's free energy.

$$\left.\frac{\partial \varepsilon}{\partial H}\right|_{H_0,\sigma_0} = -\left.\frac{\partial^2 G}{\partial \sigma \partial H}\right|_{H_0,\sigma_0} = d^{H_0,\sigma_0} \quad , \tag{20}$$

$$\left.\frac{\partial B}{\partial \sigma}\right|_{H_0,\sigma_0} = -\left.\frac{\partial^2 G}{\partial \sigma \partial H}\right|_{H_0,\sigma_0} = d^{*H_0,\sigma_0} \quad , \tag{21}$$

We use the saturation magnetization (Ms), the magnetostrictive constant (λ_{100}) and the 4th and 6th

order anisotropy constants (K_1 and K_2 respectively) to calculate the Zeeman, stress-induced anisotropy and magnetocrystalline anisotropy energies per unit volume due to a stress (σ) and a magnetic field (H) applied along the [100] direction as shown in Equations (22), (23) and (24) respectively.

$$E_H = -\mu_0 M_s H \alpha_1 , \quad (22)$$

$$E_\sigma = -\frac{3}{2}\lambda_{100}\sigma\alpha_1^2 , \quad (23)$$

$$E_{an} = K_1\left(\alpha_1^2\alpha_2^2 + \alpha_2^2\alpha_3^2 + \alpha_3^2\alpha_1^2\right) + K_2\left(\alpha_1^2\alpha_2^2\alpha_3^2\right), \quad (24)$$

The free energy (E_{TOT}) of the system corresponding to different orientations in

3D space can be expressed in terms of their direction cosines ($\alpha_1, \alpha_2, \alpha_3$) as shown in Equation (25).

$$E_{TOT}(\varphi,\theta) = E_H + E_\sigma + E_{an} , \quad (25)$$

In order to develop an expression for the bulk magnetization and magnetostriction, it is necessary to understand the following probabilistic approach. Let us assume that a bulk magnetic material is composed of a number of noninteracting magnetization units. The fraction of these units at a state (i, j), which is defined by the orientation (φ_i, θ_j) of these units, may be denoted by p_{ij} . From the physics of ferromagnetism, we know that a larger number of magnetic moments would align along a direction of lower energy. Since p_{ij} is proportional to the number of magnetic moments and inversely proportional to $E_{TOT}(\varphi_i, \theta_j)$, a probability density function given by Equation (26) can be used to express p_{ij} as a function of $E_{TOT}(\varphi_i, \theta_j)$. The choice of an exponential distribution in Equation (26) is made to avoid a singularity at E_{TOT} =0.

$$p_{ij}(\varphi_i,\theta_j) = N_m \exp\left[\frac{-E_{TOT}(\varphi_i,\theta_j)}{\Omega}\right], \quad (26)$$

where N_m is the normalizing factor which can be calculated from Equation (27) from the definition of a probability density function and is an empirical scaling factor. It is assumed that the energy is distributed in a sphere of unit radius.

$$N_m = \frac{1}{\int_{\varphi=0}^{2\pi}\int_{\theta=0}^{\pi} \exp\left[\frac{-E_{TOT}}{\Omega}\right]\left|\sin\theta\right| d\theta d\varphi} , \quad (27)$$

Let us assume $Q(\varphi,\theta)$ is a distributed physical quantity. The expected value $\langle Q \rangle$ can be obtained from Equation (28).

$$\langle Q \rangle = \frac{\int_{\varphi=0}^{2\pi}\int_{\theta=0}^{\pi} Q(\varphi,\theta)\exp\left[\frac{-E_{TOT}}{\Omega}\right]\left|\sin\theta\right| d\theta d\varphi}{\int_{\varphi=0}^{2\pi}\int_{\theta=0}^{\pi} \exp\left[\frac{-E_{TOT}}{\Omega}\right]\left|\sin\theta\right| d\theta d\varphi} , \quad (28)$$

In order to calculate the magnetization along [100], we substitute $Q(\varphi,\theta)$ with $M_{[100]}(= M_s\alpha_1)$ in Equation (28) and convert the definite integrals to finite summations which give us Equation (29). An optimum value of $\Delta\phi = \Delta\theta = 5^0$ is used for all cases to get converged solutions in reasonable computation time.

$$M = \frac{\sum_{\varphi=0}^{2\pi}\sum_{\theta=0}^{\pi} M_s\alpha_1\left|\sin\theta\right|\Delta\theta\Delta\varphi\exp\left(\frac{-E_{TOT}}{\Omega}\right)}{\sum_{\varphi=0}^{2\pi}\sum_{\theta=0}^{\pi}\left|\sin\theta\right|\Delta\theta\Delta\varphi\exp\left(\frac{-E_{TOT}}{\Omega}\right)} , \quad (29)$$

The magnetic induction is calculated using Equation (30).

$$B = \mu_0(M + H) , \quad (30)$$

The same hypothesis can be extended to calculate the magnetostriction along [100] using Equation (31).

$$\lambda = \frac{\sum_{\varphi=0}^{2\pi}\sum_{\theta=0}^{\pi} \frac{3}{2}\lambda_{100}\left(\alpha_1^2 - \frac{1}{3}\right)\left|\sin\theta\right|\Delta\theta\Delta\varphi\exp\left(\frac{-E_{TOT}}{\Omega}\right)}{\sum_{\varphi=0}^{2\pi}\sum_{\theta=0}^{\pi}\left|\sin\theta\right|\Delta\theta\Delta\varphi\exp\left(\frac{-E_{TOT}}{\Omega}\right)} , \quad (31)$$

The total strain can be described by Equation (32) where ES is the purely mechanical Young's modulus of the material and is also known as the modulus at magnetic saturation. This is the modulus measured when all the magnetic moments are oriented either parallel or anti-parallel.

$$\varepsilon = \frac{\sigma}{E_s} + \lambda , \quad (32)$$

4. Classical Beam Theory

Structural members subjected to transverse loads and operating in flexural mode are known as beams. The Euler-Bernoulli assumptions of the Classical Beam Theory are as follows.

1. The cross-section of the beam has a longitudinal plane of symmetry known as the neutral plane.

2. The resultant of the transversely applied loads lies in the longitudinal plane of symmetry.

3. Plane sections originally perpendicular to the longitudinal axis of the beam remain plane and perpendicular to the longitudinal axis after bending.

4. In the deformed beam, the planes of cross-sections have a common intersection, that is, any line originally parallel to the longitudinal axis of the beam becomes an arc of a circle described by the radius of curvature.

These assumptions are applicable to a beam whose length is 8-10 times more than both its width and its thickness.

Let us assume a beam with length (L) along the x-direction and thickness (t) along the z-direction as shown in Fig. 2, is subjected to a bending force. If the transverse displacement (w) along the z-direction after the bending deformation is much smaller than the beam thickness, then the axial displacement (u) along the xdirection can be expressed using Equation (33).

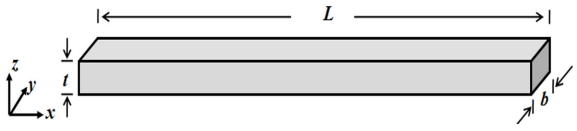

Fig. 2. An Euler-Bernoulli beam in a Cartesian coordinate system.

$$u = -z\frac{dw}{dx}, \tag{33}$$

The axial strain (ε_x) can be expressed using Equation (34):

$$\varepsilon_x = \frac{du}{dx} = -z\frac{d^2w}{dx^2}, \tag{34}$$

Using Equation (34) along with the constitutive equation ($\sigma_x = E\varepsilon_x$) for elastic material (where E is the Young's modulus of the beam material), a moment balance about the y-axis would yield Equation (35) which describes the relationship between bending moment (M), stress and beam dimensions.

$$\sigma_x = -z\frac{M}{I}, \tag{35}$$

In Equation (35), I is the 2nd moment of area which can be calculated from Equation (36) for a beam with a uniform rectangular cross-section as shown in Fig. 2.

$$I = \int_{y=-\frac{b}{2}}^{y=\frac{b}{2}} \int_{z=-\frac{t}{2}}^{z=\frac{t}{2}} z^2 dzdy = \frac{1}{12}bt^3, \tag{36}$$

The question posed at the end of the previous section motivates the study of the distribution of stress and magnetic induction along the thickness of a magnetostrictive beam which is fixed at x = 0 and free at x = L. A beam with these boundary conditions is also known as a cantilevered beam. Cantilevered beams are often used for bending characterization.

The stress at a given point in a cantilevered beam subjected to a transverse tip loading (F) can be described using Equation (37) which can be obtained by substituting $M = F(L-x)$ in Equation (35).

$$\sigma_x(x,z) = -z\frac{F(L-x)}{I} = -\frac{12FL}{bt^2}\left(\frac{z}{t}\right)\left(1-\frac{x}{L}\right), \tag{37}$$

5. Experiment Result and Discussion

Fig. 3 shows the stress distribution along the span and thickness of a cantilevered beam calculated using Equation (37). The simulation results are expressed in terms of non-dimensionalized length (x/L) and thickness (z/t). The parameters used in this calculation are F = 2 N, L = 25 mm, b = t = 1.6 mm.

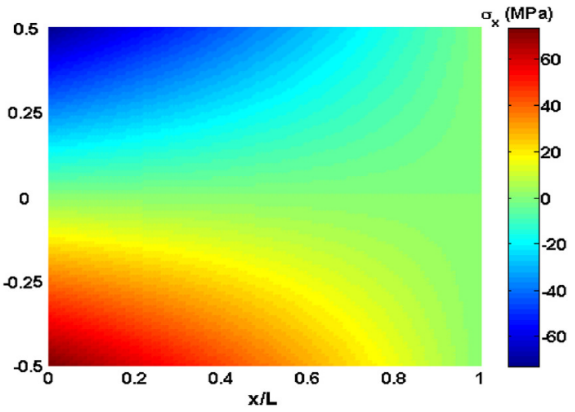

Fig. 3. Stress distribution in a cantilevered beam.

Using this stress the magnetic induction distribution in a Galfenol beam can be simulated as shown in Fig. 4. Note that B varies significantly along the span as well as thickness of the beam. A GMR or Hall-effect sensor placed on the surface of the beam would measure a value proportional to B at the location of the sensor. A pick-up coil wrapped around the beam would measure a thickness-averaged B.

Fig. 5 shows the simulation results of thickness-averaged B along the span of the same cantilevered beam subjected to a 2 N tip loading, for different bias magnetic fields. For the purpose of these simulations,

we assumed that the bias field is uniform inside the beam. These simulation results show that the thickness-averaged B measured by a pick-up coil may vary significantly along the beam span and hence the measurement of B will be affected by the length and position of the pick-up coil.

The thickness-averaged B can be deduced using the principle of superposition. The net B measured by the pick-up coil can be assumed to be the average of the B below the neutral axis of the Galfenol beam which is in tension and the B above the neutral axis of the beam which is in compression. The B below and above the neutral axis will be proportional to the volume fraction of magnetic moments and their orientation in these regions respectively. This information can be qualitatively deduced from the energy maps shown in Fig. 6.

Note that the magnetic fields used for simulation are internal magnetic fields in Galfenol and not the applied magnetic field. Moreover, a lumped parameter approach is used in demarcating regions with compressive and tensile stresses in the beam instead of using a detailed profile of the stress variation along the beam thickness. These assumptions are acceptable as we are only interested in understanding the physics of the behavior qualitatively.

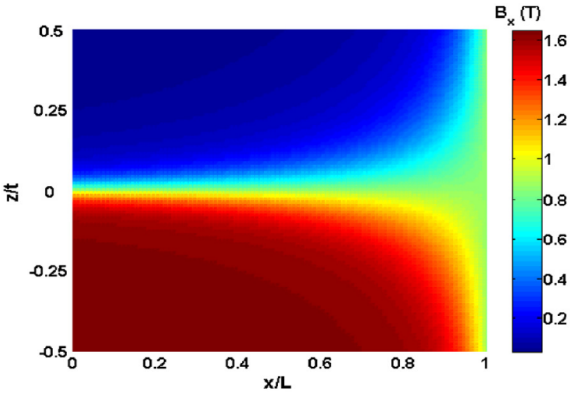

Fig. 4. Magnetic induction distribution in a cantilevered beam for a bias magnetic field of 0.5 kA/m.

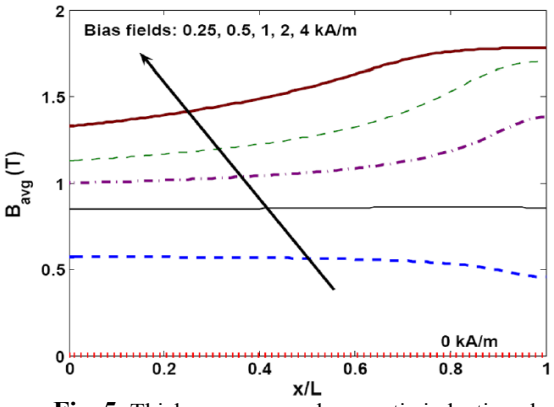

Fig. 5. Thickness-averaged magnetic induction along the span of a cantilevered beam.

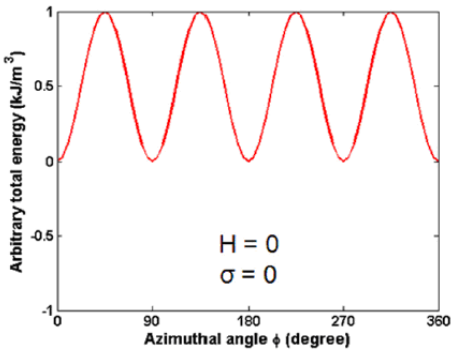

(a) in a demagnetized and un-stressed sample.

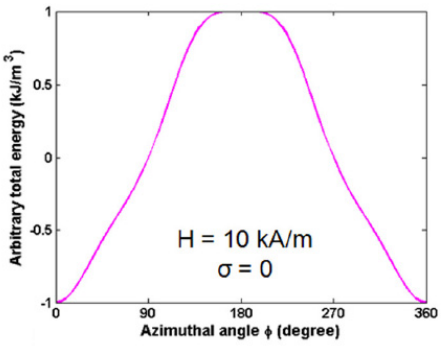

(b) after applying a high bias magnetic field.

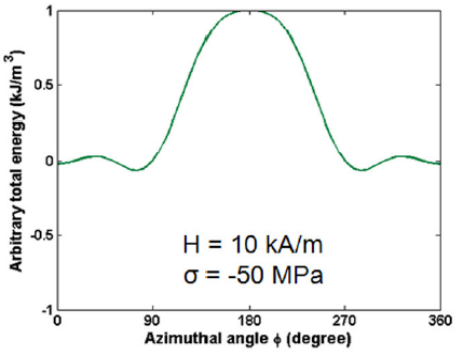

(c) in the region above neutral axis after bending.

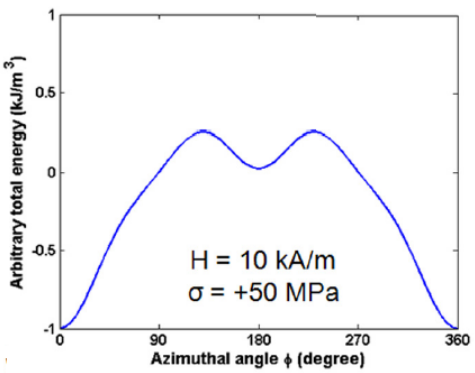

(d) in the region below neutral axis after bending.

Fig. 6. Total energy distribution in the azimuthal plane.

Fig. 6 (a) shows the four equal energy minima in Galfenol in the absence of stress and magnetic field owing to its cubic magnetocrystalline anisotropy. Fig. 6 (b) shows that when a large bias magnetic field is applied along 0°, most of the magnetic moments which were earlier oriented along 90°, 180° and 270° rotate towards 0°. When the Galfenol sample undergoes bending in presence of the large bias field, the parts of it which are in compression and tension have the energy distribution as shown in Fig. 6(c) and Fig. 6(d) respectively. The compressive stress rotates some of the magnetic moments lying above the neutral axis of the beam from 0° toward 90° and 270°. The tensile stress can rotate the magnetic moments lying below the neutral axis of the beam to either 0°. Since most of the magnetic moments are already oriented along 0° under the influence of a large bias field, the tensile stress has no effect. As a result, the effect of compressive stress in the upper half of the beam dominates over the effect of tensile stress in the beam's lower half, and a net change in thickness-averaged B is observed before and after bending in the presence of a large bias magnetic field.

6. Conclusions

This article investigates the performance analysis of Galfenol-driven cantilever beam. A magnetostrictive cantilever beam model is established, constitutive relations that describe the material behavior are based on energy minimization techniques. The Euler-Bernoulli assumptions of the Classical Beam Theory is used to solve stress of the magnetostrictive beam. Experiments and simulations are conducted to study performance of the cantilever. The sensing is primarily due to the dominating effect of compression overtension.

Acknowledgements

The authors would like to acknowledge the financial support by National Natural Science Fund of China (Grant No. 51165035, 51175395 and 51161019), Youth Science Fund of Jiangxi Province (20114BAB216006).

References

[1]. Dapino, M. J., Smith, R. C. and Flatau, A. B. Structural- Magnetic Strain Model for Magnetostrictive Transducers, *IEEE Transactions on Magnetics*, Vol. 36, 200, pp. 545-556.

[2]. D. C. Jiles, Theory of the magnetomechanical effect, *Journal of Applied Physics*, Vol. 28, 1995, pp. 1537-1546.

[3]. D. P. Ghosh, S. Gopalakrishnan, Role of Coupling Terms in Constitutive Relationships of Magnetostrictive Materials, *Computers, Materials and Continua*, Vol. 1, 2004. pp. 213-227.

[4]. J. Atulasimha, A. B Flatau, A review of magnetostrictive iron–gallium alloys, *Smart Mater. Struct.*, 20, 2011, pp. 1-15.

[5]. J. Atulasimha, G. Akhras, A. B. Flatau, Comprehensive three dimensional hysteretic magnetomechanical model and its validation with experimental <110> single-crystal iron-gallium behavior, *Journal of Applied Physics*, Vol. 103, 2008.

[6]. T. V. Jayaraman, N. Srisukhumbowornchai, S. Guruswamy, M. L. Free, Corrosion studies of single crystals of iron–gallium alloys in aqueous environments Corros, *Science*, Vol. 49, Issue 40, 2007, pp. 15–27.

[7]. J. B. Restorff, M. Wun-Fogle, A. E. Clark, K. B. Hathaway, Induced Magnetic Anisotropy in Stress-Annealed Galfenol Alloys, *IEEE Transactions on Magnetics*, Vol. 42, 2006, pp. 3087-3089.

[8]. J.-H. Yoo, U. Marschner, A. B. Flatau, Preliminary Galfenol vibratory gyro-sensor design, in *Proceedings of Smart Structures and Integrated Systems*, San Diego, CA, Vol. 5764, 2005, pp. 111-119.

[9]. P. G. Evans, M. J. Dapino, State-Space Constitutive Model for Magnetization and Magnetostriction of Galfenol Alloys, *IEEE Transactions on Magnetics*, Vol. 44, 2008. pp. 1711-1720.

[10]. P. R. Downey, A. B. Flatau, Magnetoelastic bending of Galfenol for sensor applications, *Journal of Applied Physics*, Vol. 97, 2005, pp. 10R505.

[11]. R. C. Smith, M. J. Dapino, T. R. Braun, A. P. Mortensen, A homogenized energy framework for ferromagnetic hysteresis, *IEEE Transactions on Magnetics*, Vol. 42, 2006, pp. 1747-1769.

[12]. S. Datta and A. B. Flatau, Magnetostrictive Vibration Sensor based on Iron-Gallium Alloy, in *Proceedings of Materials and Devices for Smart Systems II*, Boston, MA, Vol. 888, 2005, pp. V4.9.

[13]. T. Ueno, T. Higuchi, Miniature Magnetostrictive Linear Actuator Based on Smooth Impact Drive Mechanism, *International Journal of Applied Electromagnetics and Mechanics*, Vol. 28, 2008, pp. 135-141.

[14]. W. D. Armstrong, A directional magnetization potential based model of magnetoelastic hysteresis, *Journal of Applied Physics*, Vol. 91, 2002, pp. 2202-2210.
